THE JOURNAL OF PHYSICAL CHEMISTRY A

Article

pubs.acs.org/JPCA

Concentration Effects and Ion Properties Controlling the Fractionation of Halides during Aerosol Formation

Marcelo I. Guzman,*[,†] Richa R. Athalye,[†] and Jose M. Rodriguez[‡]

[†]Department of Chemistry, University of Kentucky, Lexington, Kentucky 40506, United States

[‡]NASA Goddard Space Flight Center, Greenbelt, Maryland 20771, United States

Supporting Information

ABSTRACT: During the aerosolization process at the sea surface, halides are incorporated into aerosol droplets, where they may play an important role in tropospheric ozone chemistry. Although this process may significantly contribute to the formation of reactive gas phase molecular halogens, little is known about the environmental factors that control how halides selectively accumulate at the air−water interface. In this study, the production of sea spray aerosol is simulated using electrospray ionization (ESI) of 100 nM equimolar solutions of NaCl, NaBr, NaI, $NaNO_2$, $NaNO_3$, $NaClO_4$, and $NaIO_4$. The microdroplets generated are analyzed by mass spectrometry to study the comparative enrichment of anions (f_{X^-}) and their correlation with ion properties. Although no correlation exists between f_{X^-} and the limiting equivalent ionic conductivity, the correlation coefficient of the linear fit with the size of the anions R_{X^-}, dehydration free-energy ΔG_{dehyd}, and polarizability α, follows the order: $R_{X^-}{}^{-2} > R_{X^-}{}^{-1} > R_{X^-} > \Delta G_{dehyd} > \alpha$. The same pure physical process is observed in H_2O and D_2O. The factor f_{X^-} does not change with pH (6.8−8.6), counterion (Li^+, Na^+, K^+, and Cs^+) substitution effects, or solvent polarity changes in methanol− and ethanol−water mixtures ($0 \le x_{H_2O} \le 1$). Sodium polysorbate 20 surfactant is used to modify the structure of the interface. Despite the observed enrichment of I^- on the air−water interface of equimolar solutions, our results of seawater mimic samples agree with a model in which the interfacial composition is increasingly enriched in $I^- < Br^- < Cl^-$ over the oceanic boundary layer due to concentration effects in sea spray aerosol formation.

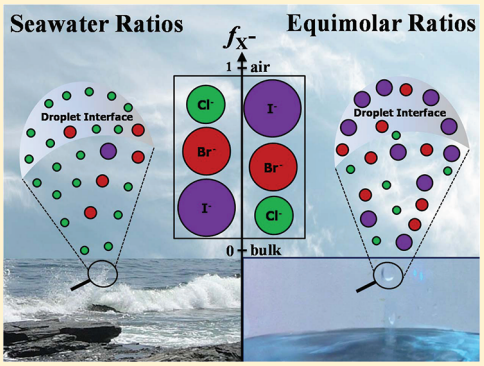

INTRODUCTION

The fractionation of species occurring at the air−water interface of the ocean is an intriguing problem and the focus of continuous experimental and theoretical studies that aim to understand the fundamental role of aerosols and their effect in radiative forcing.[1−7] The process of seawater aerosolization during bubble bursting generates negatively charged droplets (for diameters between 0.2 and 2.5 μm)[8] and establishes a negative current of ions into the atmospheric boundary layer.[9,10] Many key processes related to the transfer of anions such as halides (e.g., sea salt formation) and activation of halogens such as Br_2 to participate in the photochemical depletion of tropospheric ozone remain poorly understood.[11] The depletion of tropospheric O_3(g) molecules in the polar regions[12,13] has been linked to interfacial reactions that convert inert halide ions (e.g., Br^-) into molecular halogens (e.g., Br_2 and I_2) and reactive halogen species, RHS (e.g., $Br^•$, $BrO^•$, and $IO^•$). Once generated, RHS deplete ozone ($[O_3] \approx 40-60$ ppbv) in the Arctic boundary layer to ~0 ppbv.[12,14−16] A 2-fold important unsolved question is how are salts transferred from the ocean and then oxidized to become RHS in the air.[11,17]

The air−water interface enables unique reaction pathways that might be altered due to the high surface area available as compared to the bulk. It has been proposed that the affinity of larger anions toward the air−water interface results from their rejection by the medium via collective dispersive interactions.[18,19] Recently, a new theory that takes into account all the moments of the ionic charge distribution, and not just the dipole, predicted that larger anions are adsorbed at the interface, while the metal cations are repelled from it.[20] Simulations at higher concentrations can be interpreted in terms of ion-specific ion−surface and ion−ion excluded volume correlations.[21] Computational methods coupled with experimental results showed that, for dilute bulk concentrations, soft, polarizable monovalent anions such as I^- have a tendency to be present at the interface due to the dipole−induced dipole interaction.[22,23] Recently, electrospray ionization (ESI) mass spectrometry (MS) in the negative mode was proven to be a useful technique to study the accommodation of anions at the interface, and chemical reactions occurring during the formation of aerosol mimics.[18,24−27] Studies for >100 μM solutions described the size dependent fractionation of the outermost layers of aerosolized droplets using an ESI probe, for ions with mass to charge detection limit $m/z > 50$ amu.[18,24] In consequence, smaller anions such as chloride and nitrite have not been studied so far. Several mechanisms have been

Received: February 3, 2012
Revised: May 14, 2012
Published: May 16, 2012

proposed to control the selective enrichment of anions at the air−water interface. The mechanisms are not independent and include factors such as (1) ion size,[20,24] (2) ion polarizability,[22] and (3) ion dehydration free energy.[18,28]

In this article, we study the distribution of seven monovalent anions upon ESI aerosolization, for 100 nM equimolar solutions, what is 1000 times more diluted than previously tested,[18,24] as well as in mixtures that mimic their actual composition in seawater.[29−33] The fractionation of the environmental relevant and small Cl^- and NO_2^- ions is monitored for the first time simultaneously with Br^-, NO_3^-, I^-, ClO_4^-, and IO_4^-. The process is studied at the interface of water, D_2O, water−methanol, and water−ethanol mixtures, which are largely covered by −OH, −OD, $-CH_3$, and $-CH_2CH_3$ groups, respectively.[34−37] The use of nonionic polysorbate 20 surfactant provides direct physical insight to understand the effect of polarizability (α) above the critical micelle concentration (CMC). We show that anion fractionation in micrometer size droplets depends on the actual concentration ratios of the species present in surface ocean waters. This work also suggests that the reciprocal square of ion radius can be used as a better predictor for the enrichment of anions and that the process at relevant salts molar ratio is still dependent on ion size.

EXPERIMENTAL SECTION

Chemicals. Sodium salts were chosen to study the fractionation of anions at the air−liquid interface during the aerosolization process: NaCl (99%), NaI (99.99%), and $NaNO_2$ (99%, all from Fisher Scientific); $NaIO_4$ (99%) and NaBr (99.5%, both from Acros Organics); and $NaNO_3$ (99%) and $NaClO_4$ (99.8%, both from MP Biomedicals). In addition, potassium, lithium, and cesium halide salts were used to study the effect of cation substitution during aerosolization: KCl (99%), LiI (99%), and CsCl (99.9%, all from MP Biomedical); LiCl (>98%) and LiBr (99%, both from Alfa Aesar), CsBr (99.9%) and CsI (99.9%, both from Acros Organics); KBr (99%, Aldrich); and KI (99%, BDH Chemicals).

Preparation of Solutions. A 1.00 mM stock solution of each salt was freshly prepared daily by direct weighing and dissolution in a calibrated volumetric flask. The stock solutions were used to prepare 400 nM equimolar mixtures that underwent a 4 time dilution during infusion to a final concentration of 100 nM in each anion (unless indicated otherwise). Solutions were prepared in ultrapure water provided by an Elga Purelab flex (Veolia) water-polishing system (18.2 MΩ cm, <5 ppb organics (TOC), <1 CFU/mL), D_2O (99.9%, Cambridge Isotope), methanol (99.9%, Fisher Optima), and ethanol (99.5%, Sigma Aldrich).

Equimolar solutions in water were used to study the dependence of fractionation on (1) concentration, (2) acidity ($6.8 \leq pH \leq 8.6$), (3) solvent polarity with alcohol mixtures ($0 \leq x_{H_2O} \leq 1$), and (4) the presence of 10^{-8}−10^{-3} M polysorbate 20 (100%, Sigma Aldrich) as a nonionic surfactant. Samples at representative concentration of monovalent anions in surface seawater[29−33] were prepared.

The pH of a 1 L solution in water, with 100 nmoles of each sodium halide studied, initially at 5.96, was adjusted by the addition of 1.000×10^{-1} M NaOH (Acros Organics) and measured with a pH meter (Mettler Toledo) calibrated at pH 4.01 and 7.00 or 7.00 and 10.01 with buffer solutions (Orion).

ESI-MS Description. The process of ESI has been efficiently used for many years as a mechanism of aerosolization of nonvolatile molecules such as highly polar, ionic, and macromolecular analytes, into the gas-phase region of a mass spectrometer.[38] In our ESI system (Scheme 1), the dissolved

Scheme 1. Electrospray Ionization Mass Spectrometer (ESI-MS) Diagram

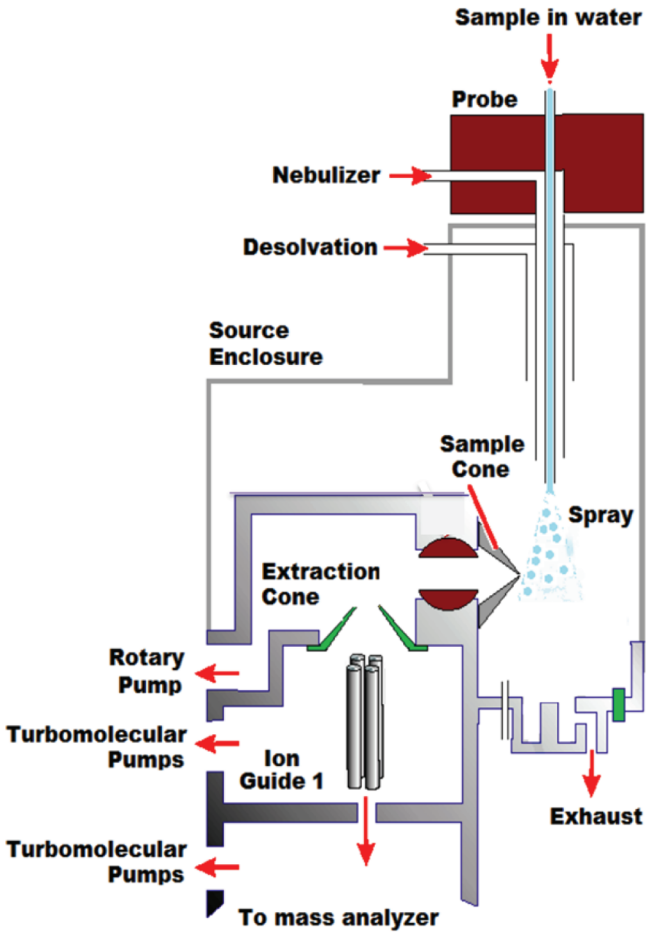

ionic compounds start their journey to the surface in a liquid solution (H_2O, D_2O, H_2O/CH_3OH, or H_2O/CH_3CH_2OH mixtures) that is nebulized into an atmospheric pressure ion source region. Pneumatically assisted electrospray converts the solution into small droplets by the combination of a strong electric potential (1.5 kV) between needle (a stainless steel capillary with 127 μm ID and 230 μm OD) and counter electrode and a high-flow of N_2 nebulizing gas (P = 70 psi, flow = 12 L min^{-1}). The capillary carrying the sample and solvent molecules is surrounded by two concentric tubes carrying the nebulizing gas; the first one (330 μm ID) assists in the aerosolization, and the second tube transports the sheath gas to help in the desolvation process of the liquid jet. The larger velocity of the N_2 nebulizing gas ($\nu_{gas} = 3.12 \times 10^4$ cm s^{-1}) over the liquid forming the plume of droplets (ν_{liquid} = 26.3 cm s^{-1}) contributes to the formation of fine aerosol droplets. The operation of the ESI probe in the negative-ion mode generates small negatively charged parent droplets with radius R_d, which subsequently form a plume of solvated molecular ions that travel between the needle and the entrance cone that acts as a counter electrode. Neutral solvent molecules undergo evapo-

dx.doi.org/10.1021/jp3011316 | J. Phys. Chem. A 2012, 116, 5428−5435

ration from the surface of the charged droplets, causing the droplets to shrink in size, shortening the distance of the negative charges at the surface of the newly formed smaller droplets. Thus, the ions are sputtered off the surface as the charge builds up, making the experiment surface sensitive.[24] The first generation daughter droplets of smaller size with a radius R_m experience charge crowding on the surface that generates repulsion forces that overcome the surface tension of the liquid. In consequence, the parent droplets disintegrate into daughter microdroplets that are 10 times smaller as indicated by the ratio $R_m/R_d < 0.1$. The ionized species are attracted toward the lower pressure orifice of the entrance cone set to −80 V, that as a counter electrode also attracts the ions. The ions travel into the first vacuum stage through the entrance capillary, where the majority of desolvation takes place and, finally, to a quadrupole mass analyzer (accurate to 0.17 amu), where they are detected at specific m/z ratios. The overall time from the formation of original droplets until ion detection is <1 ms. The extracted ion count at the specific m/z of interest showed a direct correlation with concentration. However, converting the ion count into a fractionation ratio yields a concentration independent variable that reports the behavior of the ions on the interface rather than in the bulk of the solution.[18,24]

The nebulizer voltage of the ESI probe was optimized to 1.5 kV for maximum ion count, within a range that showed the same fractionation behavior for all the ions. The cone voltage, capable of producing collisional induced dissociation (CID) of the ions, was optimized to −80 V to obtain the highest ion count for all the ions of interest; although IO_4^- could be converted to IO_3^- at this voltage, its <5% loss is considered minor. In summary, the experimental conditions were (unless indicated otherwise in a figure) drying gas temperature, 250 °C; nebulizer voltage, −1.5 kV; cone voltage, −80 V; and nebulizer pressure, 70 psi. Mass spectra were acquired between 30 and 200 amu, and the peaks at m/z 35 and 37 ($^{35,37}Cl^-$), 46 (NO_2^-), 62 (NO_3^-), 79 and 81 ($^{79,81}Br^-$), 99 and 101 ($^{99,101}ClO_4^-$), 127 (I^-), and 191 (IO_4^-) were monitored.

The mass spectra recorded reflect the composition of ions that belong to the interface layers of the ESI jet at the time it is aerodynamically sheared by the nebulizer gas. Previous related studies characterized the outermost layers of aerosolized droplets using a grounded capillary (electrode) ESI probe.[18,24] However, it was shown that the behavior of conducting and nonconducting electrospray capillaries produced similar results.[39] The experimental results presented in the next section are validated by showing that the abundance of seven anions, as reflected by their MS ion count, quantified from equimolar solutions follows a normal Hofmeister sequence.[18,24] Therefore, the enrichment is not similar for each ion, as expected at the air−water interface, and the fractionation pattern is specifically affected by the addition of surfactants.

The flow of a solvent pump (Lab Alliance) at 150 μL/min, stabilized with a back pressure regulator, was mixed through a T connector with a 50 μL/min flow of the sample in a syringe pump (Harvard Apparatus, Elite Series) and directed to the ESI-MS (Thermo Scientific, MSQ Plus). The solvent background was subtracted from the mass spectrum of the sample acquired at fixed time intervals of at least two minutes. Reported data are the average of duplicate experiments.

Present experiments are also supported by confirming the lack of any kind of correlation between the current applied to the ESI capillary and the fractionation process observed. According to Kohlraush's law, each ion in the 100 nM equimolar (dilute) solution carries its portion of the total conductivity without being affected by any of the other ions.[40] No dependence is observed between the ionic limiting equivalent conductivity for each ion ($\lambda°$) and fractionation (see Supporting Information, Figure S1A). Therefore, under the conditions chosen to study the fractionation process, the major controlling factors are the fast mixing between the nebulizing gas and the liquid ($\nu_{gas}/\nu_{liquid} = 1.19 \times 10^3$) during pneumatically assisted aerosolization and the Coulomb fission of droplets showed in the results section. In addition, the same fractionation behavior for all the ions was observed for the nebulizer voltage range between 0.5 and 2.0 kV (Supporting Information, Figure S1B).

A solution composed of 1.3 mM NaI, 0.05 mM KI, and 0.02 mM CsI, in 50:50 water−2-propanol (100%, Fisher Optima) solvent, was used to calibrate the mass spectrometer within the mass range m/z 22.9898−1971.6149 amu. The calibration conditions were drying gas temperature, 350 °C; nebulizer voltage, 3 kV; cone voltage, 75 V; and nebulizer pressure, 70 psi.

RESULTS AND DISCUSSION

Experiments with Equimolar Solutions. The mass spectrum of a 100 nM equimolar solution of NaCl, $NaNO_2$, NaBr, $NaNO_3$, NaI, $NaClO_4$, and $NaIO_4$ in water is shown in Figure 1A, relative to the ion intensity of IO_4^-. The negative ions present in the solution do not display uniformity in the ion counts detected due to the process of interfacial fractionation. Fractionation enhances the concentration of IO_4^- (the most abundant ion), ClO_4^-, and I^- over NO_3^- and Br^-. Simultaneously, fractionation practically suppresses the signals of NO_2^- and Cl^-, only observed in the inset of Figure 1. The mass spectrum of Figure 1 can be normalized as an anion enrichment or interfacial fractionation, f_{X^-}, calculated from

$$f_{X^-} = \frac{I_{m/z,X^-}}{\sum I_{m/z,X^-}} \quad (1)$$

where $I_{m/z}$ is the sum of the ion count for all the isotopes of each anion X^-, e.g., $(I_{79} + I_{81})$ for Br^-, and the denominator is the total ion count (Table 1). Although the individual ions show a linear dependence of $I_{m/z}$ on concentration, f_{X^-} is independent of concentration between 50 and 200 nM, because it is a relative measurement that reflects the composition of the outermost layers of the droplets instead of the composition of the bulk solution.[18,24]

In order to classify the dominant mechanism for the selective enrichment and depression of anions in the interface, it is useful to first explore how the different ion properties affect the process. Anion size has been proposed to control f_{X^-} in related studies[18,24] that explored its dependence on ion radius (R_{X^-}) to the first power. The implication is that f_{X^-} should depend on the free energy change associated with the rejection of anions from the liquid bulk to the air−water interface through a (negative) exponential function, $f_{X^-} \propto \exp[-^{Bulk\rightarrow Interface}\Delta G/kT]$,[18] that predicts a linear correlation between $\ln f_{X^-}$ and R_{X^-}. However, the possibility of several anions interacting at the interface has been dismissed so far. From the viewpoint of anions repelling each other, the interaction energy should be inversely proportional to the square of the ion radius, and a straight line with the best overall correlation can be expected in

dx.doi.org/10.1021/jp3011316 | J. Phys. Chem. A 2012, 116, 5428−5435

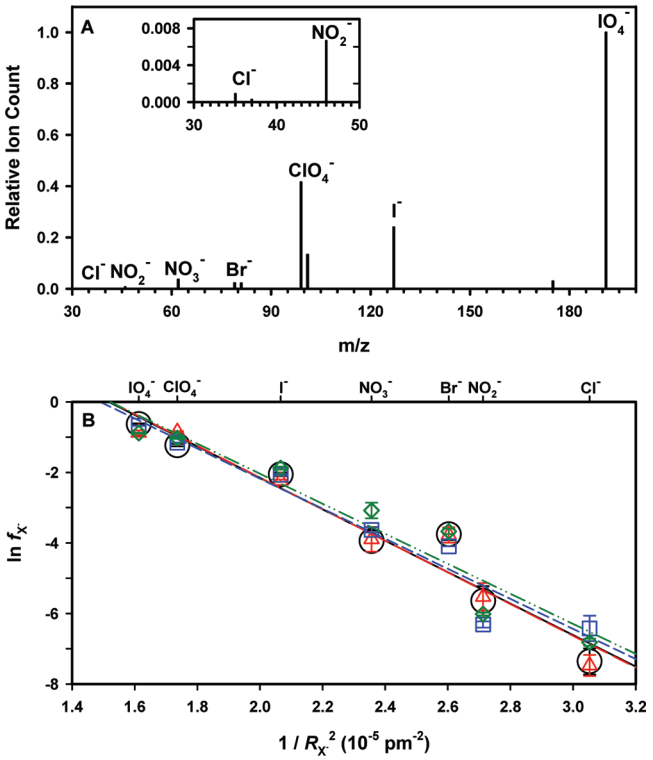

Figure 1. (A) Spectra of ESI-MS of 100 nM solution of NaCl, NaBr, NaI, $NaNO_2$, $NaNO_3$, $NaClO_4$, and $NaIO_4$ at pH 6. Ion count values normalized relative to IO_4^- count are reported in Table 1. (B) Anion fractionation factor, f_{X^-}, versus reciprocal square of anion radius (from ref 42), $R_{X^-}^{-2}$. The correlation coefficient (r^2) of the linear fit shown with dashed lines are (black open circle) 0.948 for H_2O, (red open triangle) 0.948 for D_2O, (green open diamond) 0.923 for CH_3OH, and (blue open square) 0.942 for CH_3CH_2OH.

a plot of ln f_{X^-} vs $R_{X^-}^{-2}$. Herein, we show that our experiments are better correlated with $R_{X^-}^{-2}$, what indicates that the enrichment of anions at the interface also depends on the Coulomb interactions among ions. When considering ion polarizability (α), a direct increase of f_{X^-} is expected.[41] In the case of anion dehydration free energy (ΔG_{dehyd}),[18,28] (Table 1), and given the inverse proportionality $\Delta G_{dehyd} \propto R_{X^-}^{-1}$,[42] the best correlation expected should linearly link a decrease of ln f_{X^-} with ΔG_{dehyd}.

The fact that the largest and more polarizable IO_4^- ($R_{IO_4^-}$ = 249 pm; $\alpha = 7.69 \times 10^{-30}$ m^3)[42] is the most abundant ion at the interface suggests a correlation between enrichment with anion radius (R_{X^-}) and polarizability (α). This observation agrees with the smallest and less polarizable Cl^- (R_{Cl^-} = 181 pm; $\alpha = 3.42 \times 10^{-30}$ m^3)[42] being the less enriched ion at the interface or, in other words, the most enriched ion in the solvent bulk. However, the Coulombic repulsion among anions is the controlling factor during bubble fission. Figure 1B shows the linear relationship of ln f_{X^-} vs the square of the reciprocal of anion radius ($R_{X^-}^{-2}$) for solutions in pure H_2O, D_2O, CH_3OH, and CH_3CH_2OH, respectively. The correlation of ln f_{X^-} with R_{X^-} (0.90) is smaller than with $R_{X^-}^{-2}$ (0.95) or $R_{X^-}^{-1}$ (0.93) (Figures 1 and S2, Supporting Information). Indeed, the best fitting corresponds to $R_{X^-}^{-2}$. These results reflect that the fractionation process observed is due to the Coulomb fission of microdroplets with excess negative charge and many-anion repulsion. The correlation of ln f_{X^-} with $R_{X^-}^{-2}$ and $R_{X^-}^{-1}$, indicate a dependence on Coulomb's energy and dehydration free energy (to be discussed below), respectively. It is apparent that the ratios of the linear regression slopes in Figure 1B, $m_{H2O}/m_{D_2O} = -4.46 \times 10^5$ pm^{-2}/-4.49×10^5 pm^{-2} = 0.993 and $m_{CH_3OH}/m_{CH_3CH_2OH} = -4.26 \times 10^5$ pm^{-2}/-4.27×10^5 pm^{-2} = 0.998, as well as the correlation coefficients ratios $r_{H_2O}^2/r_{D_2O}^2$ = 0.948/0.948 = 1.00 and $r_{CH_3OH}^2/r_{CH_3CH_2OH}^2$ = 0.923/0.942 = 0.980, are practically identical within experimental error. The previous observations also indicate the lack of any isotopic effect when substituting H_2O for D_2O, which is a demonstration that we are dealing with a pure physical fractionation process, where no chemical reaction is taking place, as expected in solutions of these electrolytes.

Polarizability. Figure 2 shows the ln f_{X^-} vs polarizability of the ions (α_{X^-}), which reflects the relationship between fractionation and the ability of the electronic shells of the ions to undergo deformation in an electric field.[42] The poor correlation coefficient between ln f_{X^-} and α_{X^-} ($r_{H_2O}^2$ = 0.679) is closer to the correlation between α_{X^-} and R_{X^-} ($r_{\alpha,R_{X^-}}^2$ = 0.592) also shown in Figure 2 but considerably smaller than those observed with $R_{X^-}^{-2}$ in Figure 1B. Indeed, the minor contribution of polarizability to the fractionation process can be explained by its own dependence on ion radius.

Effect of Surfactant. The effect of polysorbate 20 on anion fractionation, as nonionic surfactant, seems negligible for surfactant concentrations below 10^{-5} mol L^{-1} (Figure 3). The addition of the surfactant below the critical micelle concentration (CMC)[43] to the electrolyte solution decreases the total ion count[12] (the ion count for Cl^- vanishes); the air–water interface is altered, modifying its interfacial fractionation at even low bulk concentrations. The surfactant occupies the interface in an oriented fashion and forms micelles in the bulk phase at the CMC[43] = 8.0×10^{-5} M of polysorbate 20.[44] Figure

Table 1. Ion Properties and Fractionation of Anions at the Air–Water Interface[a]

X^-	R_{X^-} (pm)	α (10^{-30} m^3)	ΔG_{dehyd} (kJ mol^{-1})	$\lambda°$ (10^{-4} m^2 S mol^{-1})	I_{X^-}[c] (equimolar)	f_{X^-}[c] (equimolar)	f_{X^-}/f_{Cl^-}[d] (seawater)
Cl^-	181	3.42	347	76.4	1.19×10^{-3}	6.36×10^{-4}	1.00
NO_2^-	192	3.45	339	71.8	6.65×10^{-3}	3.54×10^{-3}	1.93×10^{-4}
Br^-	196	4.85	321	78.1	4.39×10^{-2}	2.34×10^{-2}	9.12×10^{-2}
NO_3^-	206[b]	4.13	306	71.5	3.63×10^{-2}	1.93×10^{-2}	9.40×10^{-4}
I^-	220	7.51	283	76.4	0.240	0.128	2.96×10^{-4}
ClO_4^-	240	5.06	214	67.4	0.549	0.292	*f*
IO_4^-	249	7.69	n.a.[e]	54.6	1.00	0.533	1.37×10^{-3}

[a]Experiments were carried out in H_2O. Key: X^-, anion; R_{X^-}, radius; α, polarizability; ΔG_{dehyd}, dehydration free energy; $\lambda°$, limiting equivalent ionic conductivity; I_{X^-}, normalized ion count; f_{X^-}, fractionation factor. R_{X^-}, α, ΔG_{dehyd}, and $\lambda°$ values are from ref 42. [b]This value corresponds to the equatorial radius. [c]Equimolar concentration data for H_2O in Figure 1. [d]Seawater molar ratio. [e]n.a., data not available. [f]Below the detection limit.

dx.doi.org/10.1021/jp3011316 | J. Phys. Chem. A 2012, 116, 5428–5435

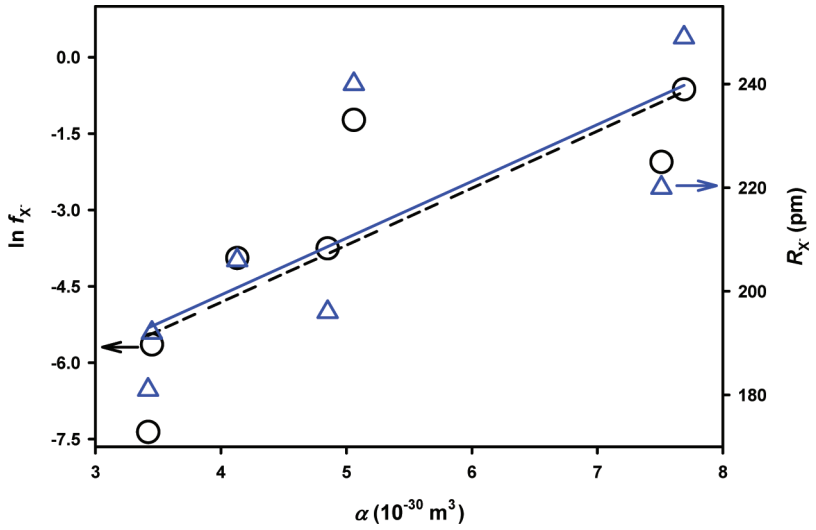

Figure 2. Anion polarizability (from ref 42) versus (black open circle) anion fractionation factors, f_X^-, and (blue open triangle) anion radius, R_X^-. The linear fit yields correlation coefficients (r^2) of 0.679 for f_X^- and 0.592 for R_X^-.

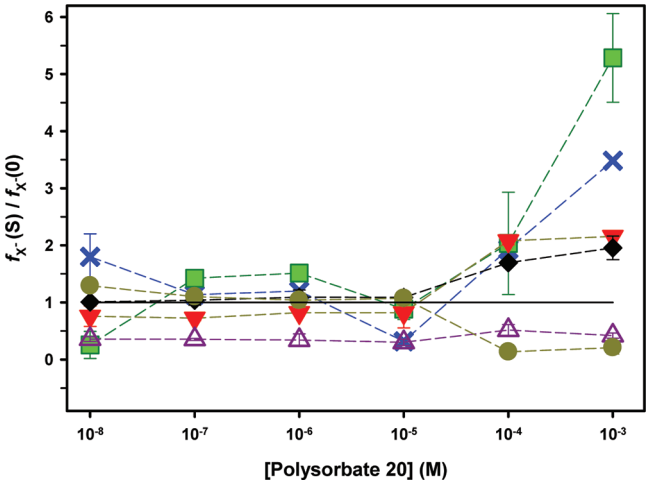

Figure 3. Ratios of anion fractionation factors in the presence and absence of surfactants, $f_X^-(S)/f_X^-(0)$, at variable concentration of polysorbate 20: (blue ×) NO_2^-, (green filled square) NO_3^-, (red filled upside-down triangle) Br^-, (black filled diamond) ClO_4^-, (purple open triangle) I^-, and (dark green filled circle) IO_4^-.

3 shows that, at low surfactant concentration, $f_{ClO_4^-}$, $f_{IO_4^-}$, and $f_{NO_2^-}$ are close to their values in water, $f(0)_{ClO_4^-}$, $f(0)_{IO_4^-}$, and $f(0)_{NO_2^-}$, while f_{I^-} and f_{Br^-} are depressed. Considerable changes are only observed for [polysorbate 20] > 10^{-5} M. At higher polysorbate 20 concentration, there is an interfacial enrichment in the population of NO_3^- > NO_2^- > Br^- > ClO_4^- in the surface layer and a fast decrease of the largest and more polarizable IO_4^- that together with I^- disturb the stability of the surface active layer. In the presence of 1 mM surfactant, the strong correlation of ln f_X^- with R_X^{-2} drops to r^2 = 0.580. Although the total population of ions (or its density) occupying the air–water interface region decreases in the presence of surfactants, the fractionation of anions that have a planar molecular geometry $f_{NO_3^-}$ and $f_{NO_2^-}$ is enhanced at the air–water interface with surfactant as compared to pure water $f_{NO_3^-}(0)$ and $f_{NO_2^-}(0)$. Other ions that show opposite behaviors at [polysorbate 20] = 10^{-3} M are ClO_4^- (enhanced) and IO_4^- (depressed) in the total number of ions still present at the interface. The opposite trend of ClO_4^- and IO_4^- is explained below.

The effect of surfactant on f_X^- can be explained in terms of salting out or salting in relative to the hydrophobic groups of polysorbate 20 in water.[43] Since the hydrophilic groups of the surfactant molecules are in contact with the aqueous phase in both the monomeric and micellar forms of the surfactant, while the hydrophobic groups are in contact with the aqueous phase only in the monomeric form, the fractionation of anions is affected by the addition of surfactant. The effects that electrolytes experience is close to be canceled out in the monomeric form below [polysorbate 20] = 10^{-5} M. Anions with low polarizability ($\alpha \leq 5.1 \times 10^{-30}$ m^3, Table 1), such as NO_2^-, NO_3^-, Br^-, and ClO_4^- are water structure makers. They salt out the hydrophobic groups of the surfactant close to the CMC and are enriched compared to those that salt in. Anions with large polarizability ($\alpha > 7.5 \times 10^{-30}$ m^3), I^- and IO_4^-, are water structure breakers; they salt in the hydrophobic groups of the surfactant and are depleted above the CMC. Thus, the enrichment ratio of anions with and without surfactant, $f_X^-(S)/f_X^-(0)$, above the CMC is affected by the polarizability and geometry of anions.[43]

Effect of Alcohols. Figure 4 shows that f_X^- measured in water–methanol and water–ethanol mixtures is only weakly dependent on the composition of the solvent for molar fractions $0 \leq x_{H_2O} \leq 1$ ($x_{R-OH} = 1 - x_{H_2O}$). Sum-frequency generation vibrational spectroscopy measurements have shown that, for increasing $x_{CH_3OH} \geq 0.2$, the dangling –OH of water gradually disappears.[35] A similar behavior is expected for ethanol.[36] The configuration includes the polar –OH group of the alcohol pointing into the bulk phase, satisfying hydrogen bonding and minimizing dipole repulsion. Independently of the surface structure tested in our experiments by gradually substituting the interfacial hydroxyl groups of water by methyl and ethyl groups,[34−37] anions selectively occupy the interface. Indeed, all anions should be oriented to minimize the distortion of the interface. Anions can repel each other and distribute in a way that provides the most gradual possible transition from the bulk solution to air. In consequence, the molecules of the

dx.doi.org/10.1021/jp3011316 | J. Phys. Chem. A 2012, 116, 5428−5435

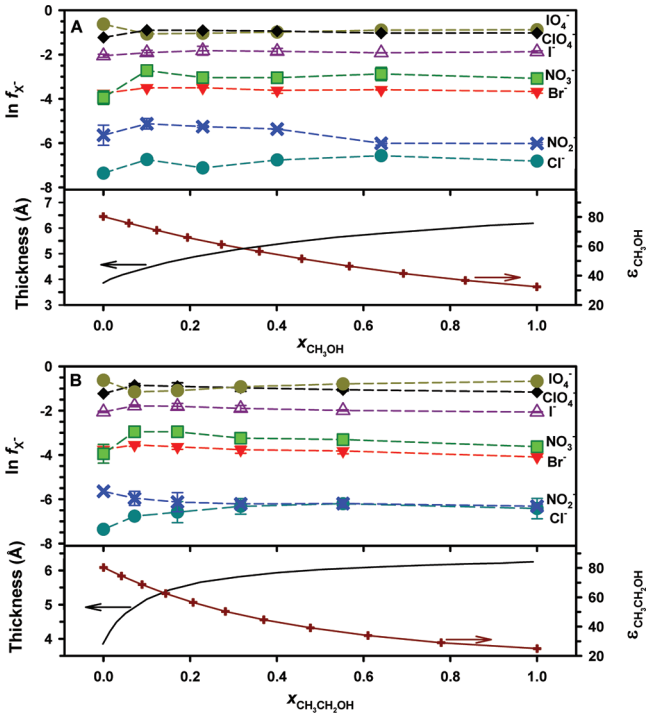

Figure 4. Anion fractionation factors, f_{X^-}, for 100 nM solution of sodium salts (top panel), interface thickness (from ref 37), and dielectric permittivity of the solvent (from ref 45), ε, (bottom panel) at variable (A) methanol and (B) ethanol molar fractions: (blue x) NO_2^-, (green filled square) NO_3^-, (red filled upside-down triangle) Br^-, (black filled diamond) ClO_4^-, (purple open triangle) I^-, (dark green filled circle) IO_4^-, and (blue-green filled circle) Cl^-.

solvent at the interface should still be oriented in a way so that their mutual interaction energy will be a maximum.[34]

For the methanol hydrophobic interface (as $x_{CH_3OH} \rightarrow 1.0$), when the surface number density reaches ~3 methanol molecules nm^{-2},[35] there is no possibility of water molecules interacting with anions, and the governing intermolecular forces involve methanol hydrogen bonding and ion-dipole interactions. The change in the interfacial layer thickness or thermal roughness with bulk concentration, evaluated as a function of the interface surface tension reported by Sung et al.,[37] is plotted in the bottom panels of Figure 4. Both water–methanol and water–ethanol interfaces have a strongly oriented outer layer, with a hydrophobic $-CH_3$ and $-CH_2-CH_3$ packing structure of thinner width than the radius of the methanol and ethanol molecules, respectively.[34,36] The fractionation factor f_{X^-} barely changes when the thickness of the outermost layer of the interface[37] is greater than ~5 Å with increasing alcohol bulk mole fraction larger than 0.2.

At the interface, a solid spherical ion of radius R_{X^-} and charge q may have one of its hemispheres submerged in the liquid bulk (a continuous dielectric medium) to a depth z and the other exposed to air.[20] The effective dielectric permittivity of the interfacial layer should gradually decrease from that of the hydrogen bonded solvent to air. Figure 4 (bottom panels) also presents the decrease in the dielectric permittivity of methanol and ethanol–water mixtures for increasing bulk alcohol molar fraction.[45] When considering the interfacial liquid slab, electrolytes strongly interact with the surrounding solvent molecules through ion–dipole interactions and occupy a position to decrease the dielectric permittivity of the solvent $\varepsilon_{solvent}$.[46] Therefore, the dielectric conductivity of the hydrated ions, ε_{X^-}, lays between the values for the interfacial layer and the solvent $\varepsilon(z)_{solvent}^{interface} < \varepsilon_{X^-} < \varepsilon_{solvent}$, where $\varepsilon(z)_{solvent}^{interface} \rightarrow \varepsilon_{air} = 1$ as $z \rightarrow 0$.[46] A competing factor to keep the ions in the bulk is their large dehydration free energy ΔG_{dehyd},[47] although its contribution seems minor ($r^2_{\ln f_{X^-}, \Delta G_{dehyd}} = 0.786$) based on the data shown in Figure S3A, Supporting Information. Atomistic simulations of ion solvation in water, dependent on the enthalpic component, suggest the surface preference of halides based on their energy minima at the surface. A partially desolvated anion favors the water–water interactions more than in the fully solvated state.[28] In addition, anion fractionation appears to be independent in the range of pH 6.8–8.6, a relevant interval for seawater, and does not change when substituting the countercation Na^+ for Li^+, K^+, or Cs^+ in 100 nM equimolar solutions containing Cl^-, Br^-, and I^- (Figure S4, Supporting Information).

Seawater Mimic Solutions of Monovalent Anions. In spite of the observed enrichment of iodide for the air–water interface of equimolar solutions, given the large concentration difference with actual seawater composition, two mimic samples of the monoanions were studied. For the first sample **I**, the concentration of sodium salts were 100 μM Cl^-, 0.44 nM NO_2^-, 1.8 nM NO_3^-, 121 nM Br^-, 41 pM I^-, 0.31 pM ClO_4^-, and 100 nM IO_4^-. All concentrations are scaled down to a reference of 100 μM Cl^-, and the molar ratios of monovalent anions in surface seawater $Cl^-/NO_2^-/NO_3^-/Br^-/I^-/ClO_4^-/IO_4^-$ were kept fixed to $100{:}4.4 \times 10^{-4}{:}1.8 \times 10^{-3}{:}0.12{:}4.1 \times 10^{-5}{:}3.1 \times 10^{-7}{:}0.10$.[29−33] The aerosolization of this sample yields f_{X^-} values (normalized to $f_{Cl^-} = 1$) for seawater molar ratios of anions (Figure S5A, Supporting Information). The experimental result shows that for actual seawater, the ratio $\gamma = f_{Cl^-}/f_{Br^-} = 26$ indicates that Cl^- is 26 times more enriched than Br^- due to its larger concentration in solution. The second seawater mimic sample **II** keeps the molar ratios for a 10-times dilution of anions in seawater, with the exception of Cl^- that is 1000 times diluted: 545 μM Cl^-, 239 nM NO_2^-, 957 nM NO_3^-, 66.24 μM Br^-, 22.2 nM I^-, 0.17 nM ClO_4^-, and 100 nM IO_4^-.[29−33] This sample was useful to confirm that Br^- becomes the second most enriched species (Figure S5B, Supporting Information). The molar ratios of anions $Cl^-/NO_2^-/NO_3^-/Br^-/I^-/ClO_4^-$ are fixed to $100{:}4.4 \times 10^{-2}{:}0.18{:}12.15{:}4.1 \times 10^{-3}{:}3.1 \times 10^{-5}$. Fractionation factors in samples **I** and **II** vary according to the change in relative concentrations.

Figure 5 shows a more realistic scenario of seawater fractionation obtained by multiplying f_{Cl^-} in sample **II** by the scaling factor γ obtained from sample **I**, where $f_{Cl^-} = 1$ means that Cl^- is by far the most enriched ion transferred to the atmosphere during bubble bursting, and $f_{Br^-} = 0.091$ accounts for Br^- being the second most enriched (9.1% of Cl^-) anion (Table 1). The bulk molar ratio $[Br^-]/[I^-] = 132$ is 2.3 times smaller than the relative excess of Br^- at the interface $f_{Br^-}/f_{I^-} = 9.10 \times 10^{-2}/2.96 \times 10^{-4} = 308$, confirming that the interfacial enrichment of I^- for equimolar solutions is not followed at relevant seawater molar ratios. Indeed, the role of concentration has to be considered in any attempt to explain the enrichment of ions at the air–water interface.

■ CONCLUSIONS

This study addresses the fundamental problem of the selective transfer of anions occurring during aerosol spray formation. The enrichment of anions at the air–water interface

dx.doi.org/10.1021/jp3011316 | J. Phys. Chem. A 2012, 116, 5428–5435

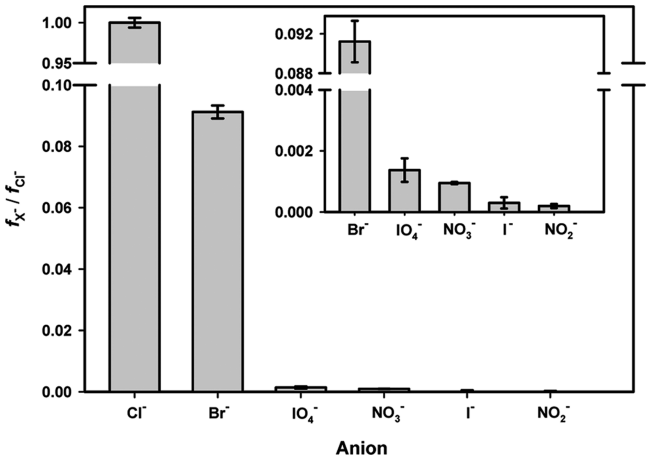

Figure 5. Anion fractionation factor, f_{X^-}, normalized relative to f_{Cl^-}, for molar ratios of anions found in seawater.

represented by the fractionation factor shows an increasing linear correlation with ion size that follows the order $R_{X^-} < R_{X^-}{}^{-1} < R_{X^-}{}^{-2}$. An explanation to the latter pattern is that the surface tension of the droplets is overcome by a series of many-body interactions among the solvated anions. These many-body interactions are stronger than the work of adhesion among solvent−solvent molecules with their associated pairwise interaction energies. The series of cascade Coulombic fission that droplets undergo, and occur a posteriori of the surface sampling stage, produce a pure physical enrichment of larger and less repulsive anions at the interface. Although the ionic limiting equivalent conductivity is not correlated with the selective enrichment of anions at the interface, minor collinearity contributions from other ion properties such as polarizability and dehydration free energy exist. The minor correlation of anion enrichment factors with polarizability can generally be explained based on the dependence of polarizability with anion size ($r_{\alpha,R_{X^-}}{}^2 = 0.592$). In addition, polarizability is not a significant predictor to be included in the model. The correlations between R_{X^-} and ΔG_{dehyd} ($r_{\Delta G_{dehyd},R_{X^-}}{}^2 = 0.960$) indicates that the combination of these ion properties to explain the trend of ln f_{X^-} represents redundant information and little can be gained by including ΔG_{dehyd} in the model. For equimolar solutions, anion enrichment factors at the air−water, air−methanol, and air−ethanol interfaces are mainly dependent on $R_{X^-}{}^{-2}$. The depletion of anion species in the presence of a nonionic surfactant above the CMC, as $[X^-]_{interface} \rightarrow 0$, follows a polarizability trend. The experimental result for seawater mimics of monovalent anions distinguishes the effect of concentration on anion enrichment factors at the air−water interface. For the latter sample, the enrichment factor ratio ($f_{Cl^-}/f_{Br^-} = 11$) is 76 times smaller than the concentration ratio of these species in seawater ($[Cl^-]/[Br^-] = 833$). Indeed, the fractionation trend observed is somewhat biased by its dependence on size as $R_{X^-}{}^{-2}$. Contrarily to the results for equimolar solutions, when the seawater molar ratios are fixed in the bulk solution, the aerosolized samples show that the air−water interface is 2.3 times richer in bromide than iodide. Present results reveal the relative position that anions occupy at the air−water interface and provide direct insight into the source of halides for the production of tropospheric RHS that participate in bromide explosion events in the early Arctic spring.

■ ASSOCIATED CONTENT

Supporting Information

Additional figures S1−S5 as mentioned in the text. This material is available free of charge via the Internet at http://pubs.acs.org.

■ AUTHOR INFORMATION

Corresponding Author

*E-mail: marcelo.guzman@uky.edu.

Notes

The authors declare no competing financial interest.

■ ACKNOWLEDGMENTS

We thank research funding from the University of Kentucky.

■ REFERENCES

(1) O'Dowd, C. D.; Jimenez, J. L.; Bahreini, R.; Flagan, R. C.; Seinfeld, J. H.; Hameri, K.; Pirjola, L.; Kulmala, M.; Jennings, S. G.; Hoffmann, T. *Nature* **2002**, *417*, 632−636.
(2) Thomas, J. L.; Jimenez-Aranda, A.; Finlayson-Pitts, B. J.; Dabdub, D. *J. Phys. Chem. A* **2006**, *110*, 1859−1867.
(3) Geddes, S.; Nichols, B.; Flemer, S.; Eisenhauer, J.; Zahardis, J.; Petrucci, G. A. *Anal. Chem.* **2010**, *82*, 7915−7923.
(4) Kwamena, N. O. A.; Buajarern, J.; Reid, J. P. *J. Phys. Chem. A* **2010**, *114*, 5787−5795.
(5) Enami, S.; Hoffmann, M. R.; Colussi, A. J. *J. Phys. Chem. Lett.* **2010**, *1*, 2374−2379.
(6) McMurdo, C. J.; Ellis, D. A.; Webster, E.; Butler, J.; Christensen, R. D.; Reid, L. K. *Environ. Sci. Technol.* **2008**, *42*, 3969−3974.
(7) Forster, P.; Ramaswamy, V.; Artaxo, P.; Berntsen, T.; Betts, R.; Fahey, D. W.; Haywood, J.; Lean, J.; Lowe, D. C.; Myhre, G.; et al. Changes in Atmospheric Constituents and in Radiative Forcing. In *The Intergovernmental Panel on Climate Change*; Cambridge University: Cambridge, U.K., 2007; Chapter 2.
(8) Reiter, R. *J. Geophys. Res., [Atmos.]* **1994**, *99*, 10807−10812.
(9) Bhattacharyya, I.; Maze, J. T.; Ewing, G. E.; Jarrold, M. F. *J. Phys. Chem. A* **2011**, *115*, 5723−5728.
(10) Blanchard, D. C. *J. Meteorol.* **1958**, *15*, 383−396.
(11) Simpson, W. R.; von Glasow, R.; Riedel, K.; Anderson, P.; Ariya, P.; Bottenheim, J.; Burrows, J.; Carpenter, L. J.; Frieß, U.; Goodsite, M. E.; et al. *Atmos. Chem. Phys.* **2007**, *7*, 4375−4418.
(12) Barrie, L. A.; Bottenheim, J. W.; Schnell, R. C.; Crutzen, P. J.; Rasmussen, R. A. *Nature* **1988**, *334*, 138−141.
(13) Carpenter, L. J.; Hopkins, J. R.; Jones, C. E.; Lewis, A. C.; Parthipan, R.; Wevill, D. J.; Poissant, L.; Pilote, M.; Constant, P. *Environ. Sci. Technol.* **2005**, *39*, 8812−8816.
(14) Liao, J.; Sihler, H.; Huey, L. G.; Neuman, J. A.; Tanner, D. J.; Friess, U.; Platt, U.; Flocke, F. M.; Orlando, J. J.; Shepson, P. B.; et al. *J. Geophys. Res., [Atmos.]* **2011**, *116*, D00R02.
(15) Hunt, S. W.; Roeselová, M.; Wang, W.; Wingen, L. M.; Knipping, E. M.; Tobias, D. J.; Dabdub, D.; Finlayson-Pitts, B. J. *J. Phys. Chem. A* **2004**, *108*, 11559−11572.
(16) Sakamoto, Y.; Yabushita, A.; Kawasaki, M.; Enami, S. *J. Phys. Chem. A* **2009**, *113*, 7707−7713.
(17) Platt, U.; Honninger, G. *Chemosphere* **2003**, *52*, 325−338.
(18) Cheng, J.; Hoffmann, M. R.; Colussi, A. J. *J. Phys. Chem. B* **2008**, *112*, 7157−7161.
(19) Bostrom, M.; Ninham, B. W. *Langmuir* **2004**, *20*, 7569−7574.
(20) Levin, Y. *Phys. Rev. Lett.* **2009**, *102*, 147803.
(21) Kalcher, I.; Schulz, J. C. F.; Dzubiella, J. *J. Chem. Phys.* **2010**, *133*, 164511.
(22) Jungwirth, P.; Tobias, D. J. *Chem. Rev.* **2005**, *106*, 1259−1281.

(23) Petersen, P. B.; Saykally, R. J. *J. Am. Chem. Soc.* **2005**, *127*, 15446−15452.
(24) Cheng, J.; Vecitis, C. D.; Hoffmann, M. R.; Colussi, A. J. *J. Phys. Chem. B* **2006**, *110*, 25598−25602.
(25) Yabushita, A.; Enami, S.; Sakamoto, Y.; Kawasaki, M.; Hoffmann, M. R.; Colussi, A. J. *J. Phys. Chem. A* **2009**, *113*, 4844−4848.
(26) Enami, S.; Hoffmann, M. R.; Colussi, A. J. *J. Phys. Chem. Lett.* **2010**, *1*, 1599−1604.
(27) Enami, S.; Stewart, L. A.; Hoffmann, M. R.; Colussi, A. J. *J. Phys. Chem. Lett.* **2010**, *1*, 3488−3493.
(28) Caleman, C.; Hub, J. S.; van Maaren, P. J.; van der Spoel, D. *Proc. Natl. Acad. Sci. U.S.A.* **2011**, *108*, 6838−6842.
(29) Stumm, W.; Morgan, J. J. *Aquatic Chemistry*, 3rd ed.; Wiley: New York, 1996.
(30) Fukushi, K.; Tada, K.; Takeda, S.; Wakida, S.; Yamane, M.; Higashi, K.; Hiiro, K. *J. Chromatogr., A* **1999**, *838*, 303−311.
(31) Fukushi, K.; Watanabe, K.; Takeda, S.; Wakida, S. I.; Yamane, M.; Higashi, K.; Hiiro, K. *J. Chromatogr., A* **1998**, *802*, 211−217.
(32) Wong, G. T. F.; Zhang, L. S. *Estuarine, Coastal Shelf Sci.* **2003**, *56*, 1093−1106.
(33) Martinelango, P. K.; Tian, K.; Dasgupta, P. K. *Anal. Chim. Acta* **2006**, *567*, 100−107.
(34) Chen, H.; Gan, W.; Lu, R.; Guo, Y.; Wang, H.-F. *J. Phys. Chem. B* **2005**, *109*, 8064−8075.
(35) Liu, W.-T.; Zhang, L.; Shen, Y. R. *J. Chem. Phys.* **2006**, *125*, 144711−144716.
(36) Gan, W.; Zhang, Z.; Feng, R.-R.; Wang, H.-F. *J. Phys. Chem. C* **2007**, *111*, 8726−8738.
(37) Sung, J.; Park, K.; Kim, D. *J. Phys. Chem. B* **2005**, *109*, 18507−18514.
(38) Cody, R. B. Electrospray Ionization Mass Spectrometry: History, Theory, and Instrumentation. In *Applied Electrospray Mass Spectrometry*, 1st ed.; Pramanik, B. N., Ganguly, A. K., Gross, M. L., Eds.; Taylor & Francis: New York, 2002; p 464.
(39) Jackson, G. S.; Enke, C. G. *Anal. Chem.* **1999**, *71*, 3777−3784.
(40) Bockris, J. O. M.; Reddy, A. K. N. *Modern Electrochemistry*, 2nd ed.; Kluwer Academic Publishers: New York, 2002; Vol. *1*.
(41) Gladich, I.; Shepson, P. B.; Carignano, M. A.; Szleifer, I. *J. Phys. Chem. A* **2011**, *115*, 5895−5899.
(42) Markus, Y. *Ion Properties*; Marcel Dekker: New York, 1997.
(43) Rosen, M. J. *Surfactants and Interfacial Phenomena*, 3rd ed.; Wiley: Hoboken, NJ, 2004.
(44) Kim, C.; Hsieh, Y.-L. *Colloids Surf., A* **2001**, *187*−*188*, 385−397.
(45) Akerlof, G. *J. Am. Chem. Soc.* **1932**, *54*, 4125−4139.
(46) Tamashiro, M. N.; Constantino, M. A. *J. Phys. Chem. B* **2010**, *114*, 3583−3591.
(47) Parsons, D. F.; Bostrom, M.; Nostro, P. L.; Ninham, B. W. *Phys. Chem. Chem. Phys.* **2011**, *13*, 12352−12367.